Simulation of Streamer Discharges Across Solid Dielectric Surfaces Using the Open-Source FEniCS Platform

T. Wong*, I. Timoshkin, S. MacGregor, M. Wilson, and M. Given
Department of Electronic and Electrical Engineering
University of Strathclyde
Glasgow, Scotland, UK
*timothy.wong@strath.ac.uk

Abstract—**Modelling the development of streamer discharges across gas-solid dielectric interfaces is of increasing importance to the power and pulsed power industries. Deeper understanding of the dynamics and morphology of fast ionisation fronts in gases and at gas-solid interfaces underpins insulation coordination and optimization in high voltage power and pulsed power systems. However, many physical mechanisms behind gas-solid flashover remain to be fully understood. In this work, an adaptive mesh drift diffusion solver implemented on the open-source finite element framework FEniCS is used to perform computational streamer modelling across gas-solid interfaces. In this study, we verify our implementation by performing studies under a published configuration of a positive streamer initiating and propagating along a flat dielectric surface in a 2D domain. FEniCS is proved fully capable of performing streamer simulations in complex gas-solid topologies, with our results providing further evidence of accelerated surface streamers and other observed effects under various initial seed positions, surface permittivity, and applied voltage magnitudes.**

Index Terms—**streamer discharges, gas-solid interface, surface flashover, drift-diffusion modelling**

I. Introduction

In high voltage power and pulsed power insulation systems, the existence of interfaces between gaseous and solid insulation is inevitable. An example includes solid dielectric spacers necessary for mechanical support in gas insulated equipment. However, due to inherent differences between the electrical characteristics of gases and solids, the breakdown behaviour of the system becomes modified due to mechanisms such as surface charge accumulation, polarisation, field redistribution, and more. Therefore, it is necessary to investigate interfacial breakdown as a separate issue from either bulk gas or bulk solid breakdown. In this work, the focus is on streamer propagation along gas-solid interfaces, whereby space charge generated by initial electron avalanches can induce sufficient local field enhancement to transition into fast propagating ionisation fronts and move through the gas. With the inclusion of nearby solid dielectrics, additional mechanisms in the form of electrostatic attraction or secondary emission may substantially affect the discharge evolution. These effects and the extent to which they modify breakdown behaviour are not yet fully understood.

In experimental studies on gas-solid flashover such as [1], authors report a reduction in the breakdown strength of nitrogen in the presence of a solid insulator, when compared to the same gap filled only with gas. In [2], similar results were reported in air, but only when the discharge travelled along the insulating surface as opposed to through the gas and slightly away from the surface. In the latter case, a higher breakdown voltage was recorded instead. A recent work [3] employed open-shutter photography to image the various discharge paths for a number of experiments using a range of solid spacer materials and gas types. In addition to discharges through the gas and along the spacer as seen in [2], the study also captured instances of discharge attachment and detachment to/from the dielectric spacer. Furthermore, the frequency of occurrence of the various types appeared to be influenced by the choice of gas, leading to the possibility that streamer mechanisms preceding the final stroke is an important factor influencing the discharge evolution. The dynamics driving these differences may have important consequences for high voltage system design and insulation coordination. Therefore, this study aims to employ computational modelling techniques to closely investigate streamers in complex gas-solid topologies.

II. Mathematical Model

A. Drift-Diffusion Equations

The problem simulated in this study mostly follows that of Li *et al.* [4], with some minor differences in the choice of transport parameters and handling of photoionization. The drift-diffusion equations for electrons (1), positive ions (2), and negative ions (3) are coupled to the Poisson equation (4) under the electrostatic assumption. The system of equations describes the temporal and spatial evolution of the charge densities and electric potential, and may be written:

$$\frac{\partial n_e}{\partial t} + \nabla \cdot (n_e \mu_e \nabla \varphi) - \nabla \cdot (D_e \nabla n_e) = S_e \qquad (1)$$

$$\frac{\partial n_+}{\partial t} - \nabla \cdot (n_+ \mu_+ \nabla \varphi) = S_+ \qquad (2)$$

$$\frac{\partial n_-}{\partial t} - \nabla \cdot (n_- \mu_- \nabla \varphi) = S_- \qquad (3)$$

$$\nabla \cdot (\varepsilon \nabla \varphi) = -q_e (n_+ - n_e - n_-) - \sigma_s (t) \qquad (4)$$

where n is the charge density in m^{-3}, μ is the electron mobility in m^{2}V^{-1}s^{-1}, D is the electron diffusion coefficient in m^{2}s^{-1}, φ is the potential in Volts, S is the summed source term over all charge densities, ε is the permittivity of the medium and $\sigma_s(t)$ is the mapped surface charge present on a dielectric surface in Cm^{-2}. The computation of the surface charge is described in section II(B). Subscripts e, $+$, and $-$ refer to electrons, positive ions, and negative ions, respectively. Processes which are considered include impact ionisation, electron attachment, photoionization, electron-ion recombination, and ion-ion recombination. Thus, the source terms are:

$$S_e = n_e(\alpha - \eta)|\mu_e \nabla \varphi| + S_{ph} + S_{se} - n_e n_+ \beta_{e+} \qquad (5)$$
$$S_+ = n_e \alpha |\mu_e \nabla \varphi| + S_{ph} - n_e n_+ \beta_{e+} - n_+ n_- \beta_{+-} \qquad (6)$$
$$S_- = n_e \eta |\mu_e \nabla \varphi| - n_+ n_- \beta_{+-} \qquad (7)$$

where α and η are the ionisation and attachment coefficients in m^{-1}, and β is the recombination coefficient subscripted $e+$ for electron-positive ion, $e-$ for electron-negative ion, and $+-$ for ion-ion recombination in m^{3}s^{-1}. S_{se} is the source term due to secondary emission, and S_{ph} is the photoionization source term in m^{-3}s^{-1}, the method from which this is computed is described in section II(C).

B. Computation of Surface Charge

To determine the surface charge accumulated on the dielectric surface, the same strategy as used in [4] was followed in the present study. The surface charge $\sigma_s(t)$ is related to the surface-directed charge density fluxes according to:

$$\frac{\partial \sigma_s(t)}{\partial t} = -q_e \left[\vec{\Gamma}_e + \vec{\Gamma}_i^- + (1 + \gamma_i)\vec{\Gamma}_i^+ + \vec{\Gamma}_{pe} \right] \qquad (8)$$

where each flux term, in order from left to right, corresponds to electrons, negative ions, positive ions, and the photoemissive flux, respectively. Here, γ_i is the secondary emission coefficient of the surface. The incident fluxes are then computed following:

$$\vec{\Gamma}_i \cdot \hat{\mathbf{n}} = a \, \text{sgn}(q_i) n_i \mu_i \vec{\mathbf{E}} \cdot \hat{\mathbf{n}} \qquad (9)$$

where a depends on the direction of the flux, ensuring only surface-directed components contribute:

$$a = \begin{cases} 1, & \text{sgn}(q_i)\mu_i \vec{\mathbf{E}} \cdot \hat{\mathbf{n}} > 0 \\ 0, & \text{sgn}(q_i)\mu_i \vec{\mathbf{E}} \cdot \hat{\mathbf{n}} \leq 0 \end{cases} \qquad (10)$$

In the work presented here, secondary emission and photoemission are excluded for comparison purposes. Thus, $\gamma_i = 0$ and the photoemissive flux term is omitted.

C. Photoionization

In atmospheric air, photoionization arising due to the de-excitation of excited nitrogen states is thought to be a significant source of free electrons ahead of positive streamers [5]. Photoionization was included through Zheleznyak's model

[6] using a 3-term Helmholtz approximation, such that the photoelectron production rate is given by:

$$\nabla^2 S_{ph,j} - (p_{O_2}\lambda_j)^2 S_{ph,j} = -\left(A_j p_{O_2}^2 \frac{p_q}{p + p_q} \xi \frac{\nu_u}{\nu_i} \right) S_\alpha \qquad (11)$$

$$S_{ph} = \sum_j S_{ph,j} \qquad (12)$$

for j = 1,2,3. p, p_q and p_{O_2} are the total pressure, quenching pressure of nitrogen, and partial pressure of oxygen in Torr, respectively. ν_u is the impact excitation frequency for level u, and ν_i is the ionization frequency in s^{-1}, while ξ is the photoionization efficiency [7]. S_α is the source term due to ionization only, $S_\alpha = \alpha \mu_e n_e |\vec{\mathbf{E}}|$. The fitting parameters λ_j and A_j used in this work follow Bourdon $et\ al.$ [8].

III. COMPUTATIONAL CONFIGURATION

A. The FEniCS Platform

The FEniCS project [8] is a collection of open-source software packages dedicated to simplifying the numerical solving of differential equations using the finite-element method (FEM). Notable aspects which are natively supported include the unified form language (UFL) [9], allowing intuitive definition of FEM problems in compact and math-like syntax; distributed memory parallelism via the message passing interface protocol (MPI); and an easy-to-use Python interface to C++ backend components, enabling a low entry barrier for new users, but compromising little on computational efficiency. In this work, a custom FEniCS-based drift-diffusion solver with adaptive mesh refinement (AMR) and dynamic time-stepping has been used. While successful benchmarking studies for positive streamers in gas have previously been demonstrated, this work extends the solver capabilities to incorporate solid dielectric inclusions.

B. Computational Domain, Initial Conditions, and Boundary Conditions

The computational domain is identical to [4] and is shown in Figure 1, consisting of a 2D domain of dimensions 4×4 cm with a dielectric slab included 1 cm from the left. The anode and cathode are located at y = 4 cm and y = 0 cm, respectively, and have applied voltages of 100 kV and 0 kV unless otherwise stated. Neumann-zero boundary conditions are applied to the left and right boundaries at x = 0 and x = 4 cm for both the potential and all charge densities. At the interface, the change in permittivity requires the electrostatic jump condition to be enforced:

$$\left(\vec{\mathbf{D}}_2 - \vec{\mathbf{D}}_1 \right) \cdot \hat{\mathbf{n}} = \sigma_s(t) \qquad (13)$$

where $\vec{\mathbf{D}}_i$ is the electric flux density in Cm^{-2} on either side of the gas-solid interface. Volume conduction has not been considered here as it is assumed to have a negligible effect over the nanosecond timescale of the simulation.

The discharge is initiated from an initially neutral seed with a capsule-like form, consisting of a rectangular body with
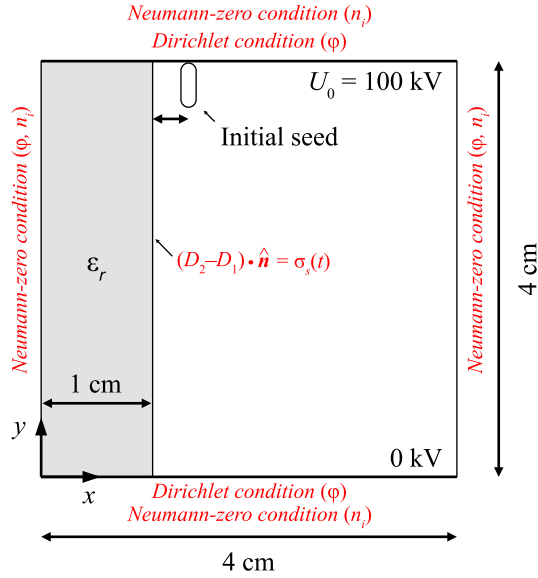
Fig. 1. Diagram of computational domain, boundary conditions, and initial seed using in the present study. Diagram adapted from [4].

Fig. 2. Time evolution of streamer electron density initiated at various initial distances. Equipotential lines are spaced by 2 kV.

Fig. 3. (*top panel*) Maximum electric field over time for streamers initiated at various initial distances. (*bottom panel*) instantaneous streamer velocity over time for $d = 0.5$ mm and 2 mm.

hemispherical ends. The length of the seed is approximately 2 mm, with a maximum electron and positive ion density of 5×10^{18} m^{-3}, placed near the anode at $d = 1$ mm away from the dielectric, unless otherwise specified. The exact definition of the seed geometry can be found in [4].

C. Transport Parameters

The gas under study is air at standard temperature and pressure (STP) conditions. For electron transport, empirical expressions fitted by Liu *et al.* [10] have been used. Ionic mobilities for both positive and negative species have been assumed to be constant at $\mu_- = \mu_+ = 3 \times 10^{-4}$ m^{2}V^{-1}s^{-1}, as have recombination coefficients, $\beta_{e+} = \beta_{+-} = 2 \times 10^{-13}$ m^{3}s^{-1}.

IV. RESULTS AND DISCUSSION

A. Varying the seed position

Figure 2 shows the evolution of the electron density of streamers initiated from varying distances away from the dielectric surface. Distances of $d = 0.5$, 1 and 2 mm are shown. Considering the differences in implementation and transport parameters, the initiation, attachment, and propagation characteristics of our streamer exhibits qualitative and quantitative agreement with [4]. For distances of $d > 2$ mm, the electrostatic attraction of the streamer toward the surface becomes increasingly weak, and it does not contact the surface within the 20 ns simulation time. The maximum electric field for streamers which do not contact the surface are near identical, as shown in Figure 3. For those that do, the time of contact is made evident by a significant increase in the maximum field strength located at the streamer head, and an increase in propagation velocity. We remark that our simulations resulted in more diffuse streamers than [4], which is likely down to the choice of electron diffusion coefficient.
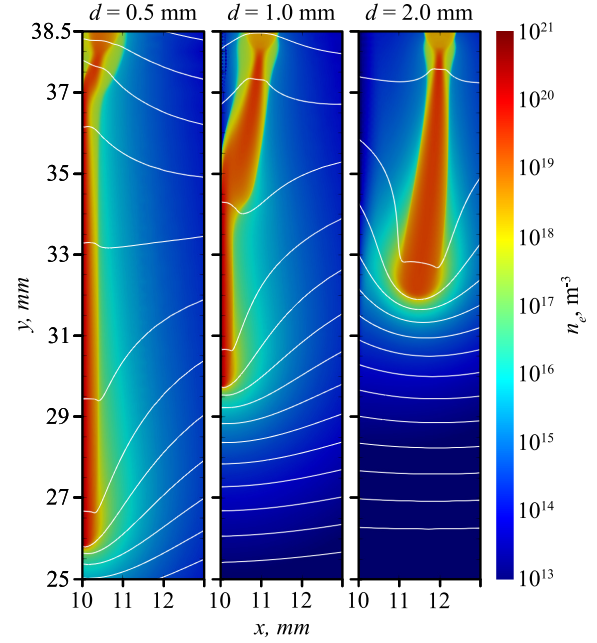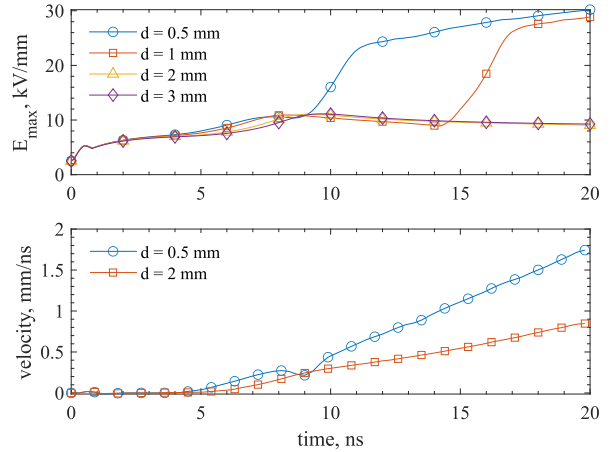
B. Varying the relative permittivity

In Figure 4, the effects of changing the surface relative permittivity on the streamer propagation are shown. While Li *et al.* [4] originally placed the seed at $d = 0.5$ mm, our seed is placed at $d = 1$ mm. Despite this, the main characteristics from both studies under varying permittivity are in agreement. We similarly observe earlier attachment with increasing surface permittivity and a higher electric field at the streamer head, leading to increased propagation velocity (Figure 5). However, for $t > 15$ ns, we observe some fluctuations in streamer velocity which are possibly numerical artefacts, requiring further investigation to confirm. The thinning of the streamer channel with higher permittivity further agrees with [4].
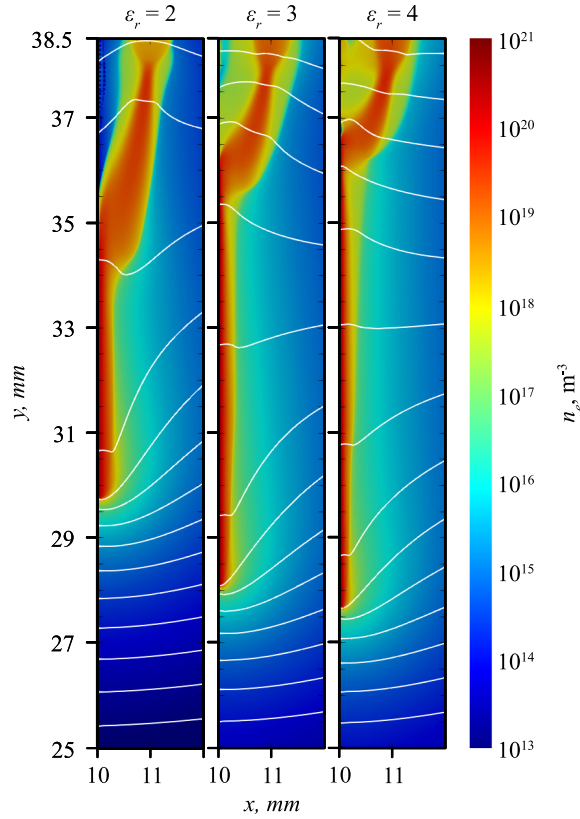
Fig. 4. Time evolution of streamer electron density initiated with various surface relative permittivity. Equipotential lines are spaced by 2 kV.
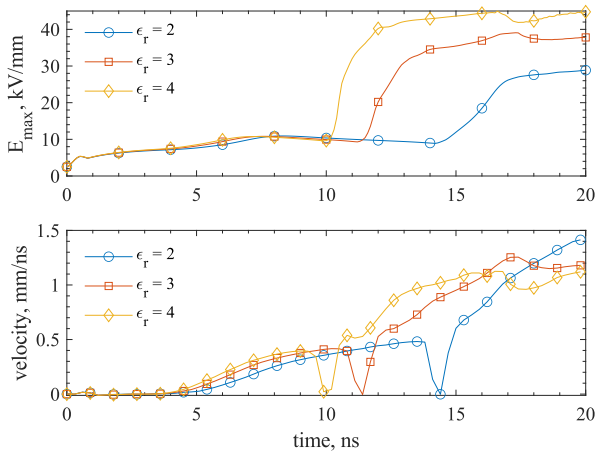

Fig. 5. (*top panel*) Maximum electric field over time (*bottom panel*) instantaneous velocity over time for streamers initiated with various surface relative permittivity.

C. Varying the applied voltage magnitude

The applied voltage magnitude was varied from 90 kV to 105 kV in 5 kV steps. This corresponds to background fields of 2.25, 2.375, 2.5 and 2.625 kVmm^{-1}, respectively. The streamers were initiated from $d = 0.5$ mm such that they attach sooner to the dielectric. In Figure 6, the moment at which the maximum field strength exhibits a rapid increase indicates the
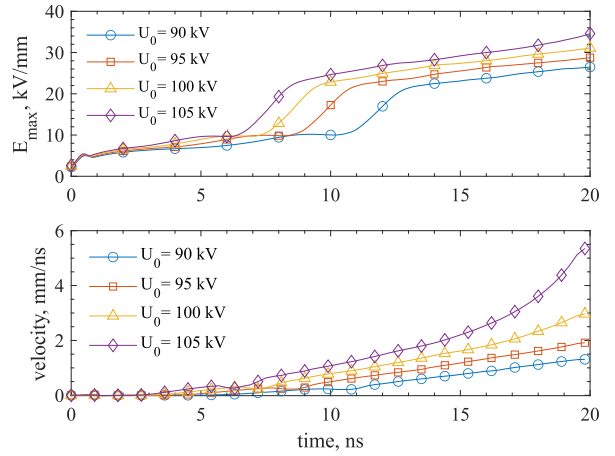

Fig. 6. (*top panel*) Maximum electric field over time (*bottom panel*) instantaneous velocity over time for streamers initiated with various applied voltages.

earlier attachment of the streamer at higher voltages, and a higher maximal field after attachment is observed. The corresponding colour plots of the electron density are shown in Figure 7. This is reflected in the streamer velocity, where higher applied voltage led to higher velocity both in the gas and on the surface. However, the acceleration of the streamer after attachment appears to be only weakly dependent on the applied voltage, as each streamer increases in velocity at a very similar rate regardless of the applied voltage. For the 105 kV case, the velocity increases rapidly beyond $t \sim 15$ ns because of the streamer's close approach to the cathode, which caused stronger field enhancement at its head and led to the observed acceleration.

V. CONCLUSION

To conclude, modifications and extensions to the open-source FEniCS code for streamer simulation has enabled the additional inclusion of solid dielectric surfaces. In this work, the accuracy of the FEniCS code was verified through comparison to an existing study of a positive streamer attaching to a solid dielectric surface. The resulting streamer characteristics under varying initial seed location, surface permittivity, and applied voltage magnitude are all in agreement with the original work, considering the differences in implementation and in the utilised transport parameters. The custom developed FEM code provides the opportunity for further investigation of streamer discharges in complex gas-solid topologies. Possible future additions include the effects of secondary emission, photoemission, pre-set surface charge, curved electrode topologies, or irregular dielectric geometry. Currently, the various component parts of the code are under continual optimisation, to ensure that modules such as AMR and time-stepping are performed as efficiently as possible. Overall, it is hoped to be used to gain deeper insights into streamer breakdown in systems relevant to pulsed power applications.
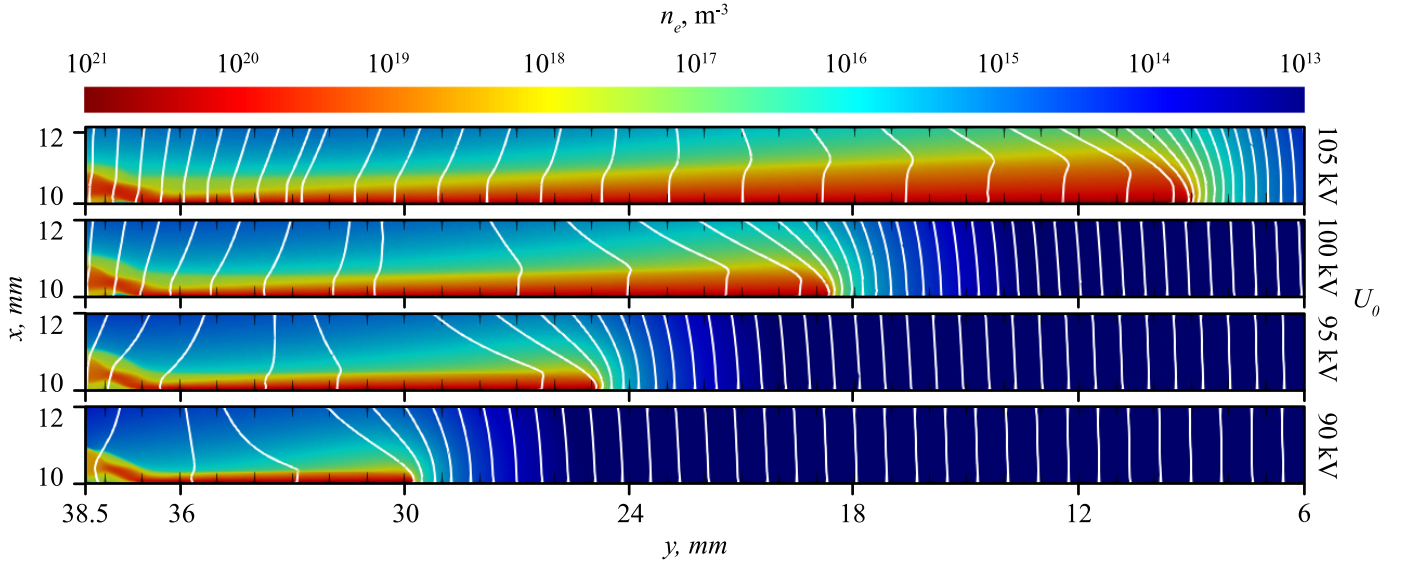
4

n_e, m^{-3}

Fig. 7. Time evolution of streamer electron density initiated with various applied voltages. Equipotential lines are spaced by 2 kV.

REFERENCES

[1] J. Trump and J. Andrias, "High-voltage d-c flashover of solid insulators in compressed nitrogen," Electrical Engineering, vol. 60, no. 11, pp. 986-989, Nov. 1941.

[2] L. Lazaridis and P. Mikropoulos, "Flashover along cylindrical insulating surfaces in a non-uniform field under positive switching impulse voltages," IEEE Trans. Dielectr. Electr. Insul., vol. 15, no. 3, pp. 694-700, Jun. 2008.

[3] Z. Wang et al., "Impulsive Breakdown Characteristics of Solid-Gas Interfaces," IEEE Trans. Plasma Sci., vol. 49, no. 1, pp. 365-377, Dec. 2020.

[4] X. Li et al., "A computational study of positive streamers interacting with dielectrics," Plasma Sources Sci. Technol., vol. 29, no. 6, Jun. 2020.

[5] S. Nijdam et al., "Probing background ionization: Positive streamers with varying pulse repetition rate and with a radioactive admixture," J. Phys. D: Appl. Phs., vol. 44, no. 45, Oct. 2011.

[6] M. Zhleznyak, A. Mnatsakanyan, and S. Sizykh, "Photo-ionization of nitrogen and oxygen mixtures by radiation from a gas-discharge," High Temp., vol. 20, pp. 356-362, 1982.

[7] A. Bourdon et al., "Efficient models for photoionization produced by non-thermal gas discharge in air based on radiative transfer and the helmholtz equations," Plasma Sources Sci. Technol., vol. 16, no. 3, pp. 656-678, Aug. 2007.

[8] A. Logg, K. Mardal, and G. Wells, Automated Solution of Differential Equations by the Finite Element Method, Springer, 2012.

[9] M. Alnaes et al., "Unified Form Language: A domain-specific language for weak formulations of partial differential equations," ACM Trans. Math. Software, vol. 40, no. 2, Feb. 2014.

[10] T. Liu et al., "Field-Time Breakdown Characteristics of Air, N_2, CO_2, and SF_6," IEEE Trans. Plasma Sci., vol. 48, no. 10, pp. 3321-3331, May. 2020.